Quark Anomalous Magnetic Moments and Neutral Pseudoscalar Meson Dynamics in Magnetized QCD Matter

Chang-Yong Yang[1] and Sheng-Qin Feng[1,2,3,*]

[1] *College of Mathematics and Physics, China Three Gorges University, Yichang 443002, China*

[2] *Center for Astronomy and Space Sciences and Institute of Modern Physics, China Three Gorges University, Yichang 443002, China*

[3] *Key Laboratory of Quark and Lepton Physics (MOE) and Institute of Particle Physics, Central China Normal University, Wuhan 430079, China*

(Dated: March 21, 2025)

Abstract

We investigate the influence of quark anomalous magnetic moments (AMM) on the mass spectra of neutral pseudoscalar mesons (π, K, η, $\eta^{'}$) under external magnetic fields, finite temperatures, and quark chemical potentials using the three-flavor Nambu-Jona-Lasinio (NJL) model. By incorporating AMM at the quark level, we reveal that AMM significantly alters the magnetic field dependence of constituent quark masses, inducing first-order phase transitions for light quarks at critical fields, while strange quarks exhibit non-monotonic mass behavior. The inclusion of AMM reshapes the QCD phase diagram, suppressing chiral transition temperatures and shifting critical endpoints (CEP) toward lower μ and T. Notably, crossover transitions observed without AMM are replaced by first-order transitions under strong fields, aligning with lattice QCD predictions for IMC. For mesons, AMM triggers abrupt mass collapses and enhances flavor mixing, accelerating chiral restoration for K and η mesons via thresholds tied to strange quark masses. The $\eta^{'}$ meson, as a resonance state, shows suppressed mass growth and instability at strong fields, highlighting limitations in handling non-perturbative decay widths within the NJL framework. These findings underscore AMM critical role in reconciling effective model predictions with LQCD results, particularly in explaining IMC and phase transition dynamics.

* Corresponding author: fengsq@ctgu.edu.cn

I. INTRODUCTION

Strong magnetic fields play a pivotal role in numerous extreme physical environments. For instance, ultra-strong magnetic fields ($\sim 10^{23}G$) that may have existed in the early universe [1, 2],the extreme magnetic field environments on the surface ($\sim 10^{15}G$) and interior ($\sim 10^{18}G$) of magnetars [3, 4], and the instantaneous strong magnetic fields ($\sim 10^{18}G$) generated in relativistic heavy ion collision experiments such as RHIC and LHC [5–11].In these scenarios, the non-trivial effects of magnetic fields on quantum chromodynamics (QCD) matter have garnered widespread attention, particularly their modulation of the phase structure and dynamical behavior of strongly interacting matter. Specifically, the presence of strong magnetic fields has led to the emergence of numerous new and observable physical effects in quark matter, which contribute to a better understanding of Quantum Chromodynamics (QCD), the fundamental theory of strong interactions and considered one of the most promising theories. For instance, some of these effects involve magnetic catalysis (MC) [12] and inverse magnetic catalysis (IMC) [13] related to the dynamical chiral symmetry breaking mentioned in this article, while others involve related phenomena such as chiral magnetic effect (CME) and chiral vorticity effect (CVE) [14–16].

From a theoretical perspective, magnetic fields significantly affect the properties of QCD vacuum and matter. For instance, the magnetic catalysis (MC) effect indicates that magnetic fields can enhance chiral symmetry breaking through dimensional reduction mechanisms, leading to an increase in quark condensation and a rise in phase transition temperature [17–21].

However, lattice QCD (LQCD) simulations at finite temperatures reveal an opposite trend: near the phase transition region, chiral condensation exhibits non-monotonic behavior with increasing magnetic fields, and the phase transition temperature decreases as the magnetic field increases [16, 22–24]. This phenomenon is known as Inverse Magnetic Catalysis (IMC) [25–28]. The microscopic mechanism underlying this anomalous behavior remains incompletely elucidated, posing a significant challenge for current theoretical research.

To explain the IMC effect, researchers have proposed various phenomenological schemes, including introducing a magnetic field-dependent coupling constant in the NJL model [29–32], considering the anomalous magnetic moment (AMM) of quarks [28, 33, 34], or going beyond the mean-field approximation [35]. It is worth noting that the physical origin of

AMM is closely related to chiral symmetry breaking: studies have shown that AMM can not only be induced by an external magnetic field [36–38], but its dynamic generation mechanism may also be intrinsically linked to the magnetic catalytic effect [39–42]. Therefore, once quarks obtain dynamical mass, they should also obtain a dynamical AMM.

In recent years, the study of magnetic field effects on the hadron spectra has induced widespread attention. As Goldstone bosons with chiral (isospin) symmetry breaking, the properties of pseudoscalar mesons under finite temperatures, magnetic fields, and densities have been extensively studied [43–59]. However, existing research has mostly focused on the two-flavor NJL model, and the correlation between AMM and the mass spectrum of neutral pseudoscalar mesons in the three-flavor system has not been systematically explored, which limits the model's predictive ability for the phase structure of multi-flavor quark systems.

Based on the three-flavor NJL model, this article systematically investigates for the first time the influence of quark AMM on the mass spectra of neutral pseudoscalar mesons (π, K, η, $\eta^{'}$) under the joint regulation of magnetic field, temperature, and chemical potential. By introducing AMM at the quark level, we reveal the following key issues: (1) how AMM modifies the dependence of quark mass on magnetic field, thereby reshaping the QCD phase diagram; (2) the enhancement effect of AMM-induced flavor symmetry breaking on meson mixing (such as $\pi_0-\eta-\eta^{'}$ mixing); (3) the correlation mechanism between the abrupt change behavior of meson mass and chiral symmetry restoration under strong magnetic fields. This study not only provides a new perspective for understanding the IMC effect but also verifies the necessity of AMM in effective models by comparing with LQCD results.

The structure of the full text is as follows: Section II introduces the theoretical framework of the three-flavor NJL model with AMM; Section III presents numerical results for quark masses, phase diagrams, and meson mass spectra, and analyzes their physical implications; Section IV summarizes the main conclusions and makes discussions.

II. MODEL AND FORMALISM

The SU(3) NJL model with the AMM of quarks is defined via following the Lagrangian density under external constant magnetic field:

$$\begin{aligned}\mathcal{L}_{NJL} = &\sum_{f=u,d,s} \bar{\psi}_f(i\gamma^\mu D_\mu^{(f)} - m_f - \frac{1}{2}e_f\kappa_f\sigma^{\mu\nu}F_{\mu\nu})\psi_f + \\ &G\sum_{a=0}^{8}[(\bar{\psi}\lambda_a\psi)^2 + (\bar{\psi}i\gamma^5\lambda_a\psi)^2] - K(det[\bar{\psi}(1+\gamma^5)\psi] + det[\bar{\psi}(1-\gamma^5)\psi]),\end{aligned} \tag{1}$$

where, $\psi = (\psi_u, \psi_d, \psi_s)$ are Dirac spinor for u, d, and s quarks, respectively, λ_a with $a = 1, 2, ..., 8$ are Gell-Mann matrices with $\lambda_0 = \sqrt{\frac{2}{3}}$, m_f is the current quark mass, $D_\mu^{(f)} = \partial_\mu + iq_f A_\mu$ is the covariant derivative with quark charge $q_f = diag(\frac{2}{3}e, -\frac{1}{3}e, -\frac{1}{3}e)$, $F_{\mu\nu} = \partial_\mu A_\nu - \partial_\nu A_\mu$ is the electromagnetic field strength, κ_f denotes the AMM of quarks with flavor $f = u, d, s$. Without loss of generality, we consider the magnetic field along z direction and take Landau gauge $A_\mu = (0, 0, xB, 0)$. The last term in Eq. (1) is six-fermion Kobayashi-Maskawa-t$'$ Hooft interaction [60–64] that breaks the $U_A(1)$ symmetry.

Under the mean-field approximation, the thermodynamic potential is taken as

$$\Omega_{MF} = \Omega_q + 2G(\sigma_u^2 + \sigma_d^2 + \sigma_s^2) - 4K\sigma_u\sigma_d\sigma_s, \tag{2}$$

where

$$\Omega_q = -3\sum_{f=u,d,s}\frac{|q_f B|}{2\pi}\sum_n\sum_{s=\pm1}\int\frac{dp_z}{2\pi}[E_{fns} + T\ln\Big(1+e^{-\frac{E_{fns}+\mu}{T}}\Big) + T\ln\Big(1+e^{-\frac{E_{fns}-\mu}{T}}\Big)], \tag{3}$$

where $E_{fns} = \sqrt{p_z + (M_{nf} - s\kappa_f e_f B)^2}$, $M_{nf} = \sqrt{M_f^2 + 2n|e_f B|}$ and chiral condensates σ_f. The corresponding effective quark masses satisfies

$$M_f = m_f - 4G\sigma_f + 2K\prod_{f'=f}\sigma_{f'}. \tag{4}$$

By minimizing the thermodynamic potential $\partial\Omega_{MF}/\partial\sigma_f = 0$,one can obtain the chiral condensates $\sigma_f = <\bar{\psi}_f\psi_f>$ as

$$<\bar{\psi}_f\psi_f> = -\frac{|e_f B|}{(2\pi)^2}\int dp_z\sum_{n,s}\frac{M_f}{E_{fns}}(1 - \frac{s\kappa_f e_f B}{M_{nf}})(1 - \frac{1}{e^{(E_{fns}-\mu)/T}+1} - \frac{1}{e^{(E_{fns}+\mu)/T}+1}), \tag{5}$$

where $s = +1$ for u quark, $s = -1$ for d and s quarks, respectively, at lowest Landon level.

To obtain the expression for the meson propagator, it is necessary to introduce the self-consistent Bethe-Salpeter equation (BSE) with the random phase approximation (RPA) in

the NJL model [65–70]. Under the mean-field approximation, it is necessary to transform the six-fermion interaction into an effective four-fermion interaction [71]. The corresponding Lagrangian density can be expressed as:

$$\begin{aligned}
&\mathcal{L}_{NJL} = \sum_{f=u,d,s} \bar{\psi}_f(i\gamma^\mu D_\mu^{(f)} - m_f - \frac{1}{2}e_f\kappa_f\sigma^{\mu\nu}F_{\mu\nu})\psi_f + \\
&\sum_{a=0}^{8}[K_a^-(\bar{\psi}\lambda_a\psi)^2 + K_a^+(\bar{\psi}i\gamma^5\lambda_a\psi)^2] + \\
&K_{30}^-(\bar{\psi}\lambda_3\psi)(\bar{\psi}\lambda_0\psi) + K_{30}^+(\bar{\psi}i\gamma^5\lambda_3\psi)(\bar{\psi}i\gamma^5\lambda_0\psi) + K_{03}^-(\bar{\psi}\lambda_0\psi)(\bar{\psi}\lambda_3\psi) + K_{03}^+(\bar{\psi}i\gamma^5\lambda_0\psi)(\bar{\psi}i\gamma^5\lambda_3\psi) + \\
&K_{80}^-(\bar{\psi}\lambda_8\psi)(\bar{\psi}\lambda_0\psi) + K_{80}^+(\bar{\psi}i\gamma^5\lambda_8\psi)(\bar{\psi}i\gamma^5\lambda_0\psi) + K_{08}^-(\bar{\psi}\lambda_0\psi)(\bar{\psi}\lambda_8\psi) + K_{08}^+(\bar{\psi}i\gamma^5\lambda_0\psi)(\bar{\psi}i\gamma^5\lambda_8\psi) + \\
&K_{83}^-(\bar{\psi}\lambda_8\psi)(\bar{\psi}\lambda_3\psi) + K_{83}^+(\bar{\psi}i\gamma^5\lambda_8\psi)(\bar{\psi}i\gamma^5\lambda_3\psi) + K_{38}^-(\bar{\psi}\lambda_3\psi)(\bar{\psi}\lambda_8\psi) + K_{38}^+(\bar{\psi}i\gamma^5\lambda_3\psi)(\bar{\psi}i\gamma^5\lambda_8\psi),
\end{aligned} \tag{6}$$

where the effective coupling constants are taken as

$$\begin{aligned}
K_0^\pm &= G \pm \frac{1}{3}K(\sigma_u + \sigma_d + \sigma_s), \\
K_1^\pm &= K_2^\pm = K_3^\pm = G \pm \frac{1}{2}K\sigma_s, \\
K_4^\pm &= K_5^\pm = G \pm \frac{1}{2}K\sigma_d, \\
K_6^\pm &= K_7^\pm = G \pm \frac{1}{2}K\sigma_u, \\
K_8^\pm &= G \pm \frac{1}{6}K(2\sigma_u + 2\sigma_d - \sigma_s), \\
K_{30}^\pm &= K_{03}^\pm = \mp\frac{1}{2\sqrt{6}}K(\sigma_u - \sigma_d), \\
K_{80}^\pm &= K_{08}^\pm = \pm\frac{\sqrt{2}}{12}K(\sigma_u + \sigma_d - 2\sigma_s), \\
K_{83}^\pm &= K_{38}^\pm = \pm\frac{1}{2\sqrt{3}}K(\sigma_u - \sigma_d),
\end{aligned} \tag{7}$$

and chiral condensates are obtained as

$$\sigma_u = <\bar{\psi}_u\psi_u>, \sigma_d = <\bar{\psi}_d\psi_d>, \sigma_s = <\bar{\psi}_s\psi_s> . \tag{8}$$

We only consider neutral mesons, whose quark propagator Schwinger phase can be cancelled. For mesons that do not mix with other mesons, their propagators can be represented by polarization loops [67] through RPA as:

$$\frac{1}{i}[\Pi_{ps}(p)]_{ij} = -N_c\sum_{ff'}\int\frac{d^4k}{(2\pi)^4}tr[\gamma^5(T_i)_{ff}S^f(p+k)\gamma^5(T_j)_{ff'}S^{f'}(k)], \tag{9}$$

where the flavor indices f and f' are explicitly included and the trace corresponds to the spinor trace only, $\mathcal{S}^f$ is the quark propagator of flavor f, and the vertex of non- mixing mesons can be given as

$$T_i = \begin{cases} \frac{1}{\sqrt{2}}(\lambda_1 \pm i\lambda_2), & \text{for } \pi^{\pm} \\ \frac{1}{\sqrt{2}}(\lambda_6 \pm i\lambda_7), & \text{for } K^0, \bar{K}^0 \\ \frac{1}{\sqrt{2}}(\lambda_4 \pm i\lambda_5), & \text{for } K^{\pm} \end{cases}. \tag{10}$$

Therefore, K^0 meson propagator can be given as

$$M = \frac{2K_6^+}{1 - 2K_6^+ \Pi^{ps}_{K^0}(p)}, \tag{11}$$

and the mass is determined by solving the equation

$$1 - 2K_6^+ \Pi^{ps}_{K^0}(p_0, \vec{p} = 0) = 0. \tag{12}$$

The magnetic field can break isospin symmetry, and the AMM of quarks can even enhance this breaking effect, leading to the production of mixing states $\pi_0 - \eta - \eta'$. For the mixing mesons, the meson propagator [72] can be expressed as

$$M = \begin{bmatrix} M_{00} & M_{03} & M_{08} \\ M_{30} & M_{33} & M_{38} \\ M_{80} & M_{83} & M_{88} \end{bmatrix} = 2K^+ \left(1 - 2\Pi^{ps} K^+\right)^{-1}, \tag{13}$$

where

$$K^+ = \begin{bmatrix} K^+_{00} & K^+_{03} & K^+_{08} \\ K^+_{30} & K^+_{33} & K^+_{38} \\ K^+_{80} & K^+_{83} & K^+_{88} \end{bmatrix}, \tag{14}$$

and

$$\Pi^{ps} = \begin{bmatrix} \Pi^{ps}_{00} & \Pi^{ps}_{03} & \Pi^{ps}_{08} \\ \Pi^{ps}_{30} & \Pi^{ps}_{33} & \Pi^{ps}_{38} \\ \Pi^{ps}_{80} & \Pi^{ps}_{83} & \Pi^{ps}_{88} \end{bmatrix}, \tag{15}$$

and they satisfy the following equations$K_{03}^{+}=K_{30}^{+}, K_{08}^{+}=K_{80}^{+}, K_{38}^{+}=K_{83}^{+}$, and

$$\begin{aligned}
\Pi_{00}^{ps} &= \frac{2}{3}\left(\Pi_{u\bar{u}}^{ps}+\Pi_{d\bar{d}}^{ps}+\Pi_{s\bar{s}}^{ps}\right), \\
\Pi_{03}^{ps} &= \Pi_{30}^{ps}=\sqrt{\frac{2}{3}}\left(\Pi_{u\bar{u}}^{ps}-\Pi_{d\bar{d}}^{ps}\right), \\
\Pi_{08}^{ps} &= \Pi_{80}^{ps}=\frac{\sqrt{2}}{3}\left(\Pi_{u\bar{u}}^{ps}+\Pi_{d\bar{d}}^{ps}-2\Pi_{s\bar{s}}^{ps}\right), \\
\Pi_{33}^{ps} &= \Pi_{u\bar{u}}^{ps}+\Pi_{d\bar{d}}^{ps}, \\
\Pi_{38}^{ps} &= \Pi_{83}^{ps}=\frac{\sqrt{3}}{3}\left(\Pi_{u\bar{u}}^{ps}-\Pi_{d\bar{d}}^{ps}\right), \\
\Pi_{88}^{ps} &= \frac{1}{3}\left(\Pi_{u\bar{u}}^{ps}+\Pi_{d\bar{d}}^{ps}+4\Pi_{s\bar{s}}^{ps}\right).
\end{aligned} \tag{16}$$

The $\pi_0, \eta, \eta^{'}$ meson masses can be determined by solving the equation as

$$\det\left[M^{-1}(p_0, \vec{p}=0)\right]=0. \tag{17}$$

One can simplify the inverse of meson propagator matrix M as

$$M^{-1}=\frac{1}{2\det K^{+}}\begin{pmatrix} D & A & B \\ A & E & C \\ B & C & F \end{pmatrix}, \tag{18}$$

with

$$\begin{aligned}
A &= K_{08}^{+}K_{38}^{+}-K_{03}^{+}K_{88}^{+}-2\Pi_{03}^{ps}\det K^{+}, \\
B &= K_{08}^{+}K_{38}^{+}-K_{08}^{+}K_{33}^{+}-2\Pi_{08}^{ps}\det K^{+}, \\
C &= K_{08}^{+}K_{03}^{+}-K_{00}^{+}K_{38}^{+}-2\Pi_{38}^{ps}\det K^{+}, \\
D &= K_{33}^{+}K_{38}^{+}-(K_{38}^{+})^2-2\Pi_{00}^{ps}\det K^{+}, \\
E &= K_{00}^{+}K_{88}^{+}-(K_{08}^{+})^2-2\Pi_{33}^{ps}\det K^{+}, \\
F &= K_{00}^{+}K_{33}^{+}-(K_{03}^{+})^2-2\Pi_{88}^{ps}\det K^{+}.
\end{aligned} \tag{19}$$

It is worth emphasizing that we can obtain the meson mass through Eq. (17), where the three pairs of roots correspond to the masses of π_0, η, η' mesons. To calculate the polarization loop, we need to use the quark propagator. We can first solve the Dirac equation corresponding to the first term in Eq. (1). And then, the quark propagator is obtained by employing the standard canonical quantization in quantum field theory and the real-time formula of thermal field theory. When $n=0$, the quark propagator of the flavor f in momentum space

with the real-time formula can be obtained as [73]

$$
\begin{aligned}
S_{f0}(k) &= e^{-\frac{{k_\perp}^2}{|e_f B|}}\left[(k_0\gamma^0 - k_z\gamma^3) + (M_f - s\kappa_f e_f B)\right] \\
&\times (1 + \mathrm{sign}(e_f) i\gamma^1\gamma^2)\left\{\frac{1}{k_0^2 - {E_{f0s}}^2 + i\varepsilon} + 2\pi i n_F(k_0)\delta(k_0^2 - {E_{f0s}}^2)\right\},
\end{aligned}
\tag{20}
$$

and when $n \geq 1$, the quark propagator of the flavor f in momentum space can be given as

$$
\begin{aligned}
S_f(k) &= e^{-\frac{{k_\perp}^2}{|e_f B|}}\sum_{n,s}(-1)^n \frac{1}{2M_{nf}}\{(M_{nf} + sM_f)[(k_0\gamma^0 - k_z\gamma^3) + (sM_{nf} - \kappa_f e_f B)] \\
&\times (1 + \mathrm{sign}(e_f) i\gamma^1\gamma^2) L_n\left(\frac{2{k_\perp}^2}{|e_f B|}\right) - (M_{nf} - sM_f)[(k_0\gamma^0 - k_z\gamma^3) \\
&- (sM_{nf} - \kappa_f e_f B)](1 - \mathrm{sign}(e_f) i\gamma^1\gamma^2) L_{n-1}\left(\frac{2{k_\perp}^2}{|e_f B|}\right) \\
&- 4[(k_0\gamma^0 - k_z\gamma^3)\mathrm{sign}(e_f) i\gamma^1\gamma^2 + (sM_{nf} - \kappa_f e_f B)](-k_x\gamma^1 - k_y\gamma^2) s L_{n-1}^1\left(\frac{2{k_\perp}^2}{|e_f B|}\right)\} \\
&\times \left\{\frac{1}{k_0^2 - {E_{f0s}}^2 + i\varepsilon} + 2\pi i n_F(k_0)\delta(k_0^2 - {E_{f0s}}^2)\right\},
\end{aligned}
\tag{21}
$$

where E_{fns} represents the energy eigenvalue, L_n stands for the Laguerre polynomial of order n, the index $s = \pm 1$ denotes the spin quantum number, and $s = +1$ for u quark, $s = -1$ for d and s quarks at lowest Landau level. $n_F(k_0)$ that appears in Eqs. (20) and (21) can be obtained as

$$
n_F(k_0) = \theta(k_0)\frac{1}{e^{(k_0-\mu)/T} + 1} + \theta(-k_0)\frac{1}{e^{-(k_0-\mu)/T} + 1}. \tag{22}
$$

For kaon meson, the polarization loop can be obtained as

$$
\begin{aligned}
\Pi_{K^0}^{ps}(p_0 = m_{K^0}) &= \frac{\beta N_c}{2(2\pi)^2}\sum_{n,s,l}(1 + sl\frac{M_d M_s + 2\beta n}{M_{nd} M_{ns}}) \\
&\times \left\{\int dk_z \frac{1}{E_{dns}}\left[1 - \frac{1}{e^{(E_{dns}-\mu)/T} + 1} - \frac{1}{e^{(E_{dns}+\mu)/T} + 1}\right]\right. \\
&+ \int dk_z \frac{1}{E_{snl}}\left[1 - \frac{1}{e^{(E_{snl}-\mu)/T} + 1} - \frac{1}{e^{(E_{snl}+\mu)/T} + 1}\right] \\
&\left. + \left\{[(M_{nd} - s\kappa_d e_d B) - sl(M_{ns} - l\kappa_s e_s B)]^2 - p_0^2\right\} B(m_d, m_s)\right\},
\end{aligned}
\tag{23}
$$

where

$$
\begin{aligned}
&B(m_d, m_s) = \\
&\int dk_z \left\{\frac{1}{E_{dns}}\left[\frac{1}{(E_{dns} + p_0)^2 - {E_{snl}}^2}\frac{1}{e^{-(E_{dns}+\mu)/T} + 1} - \frac{1}{(E_{dns} - p_0)^2 - {E_{snl}}^2}\frac{1}{e^{(E_{dns}-\mu)/T} + 1}\right]\right. \\
&\left. + \frac{1}{E_{snl}}\left[\frac{1}{(E_{snl} - p_0)^2 - {E_{dns}}^2}\frac{1}{e^{-(E_{snl}+\mu)/T} + 1} - \frac{1}{(E_{snl} + p_0)^2 - {E_{dns}}^2}\frac{1}{e^{(E_{snl}-\mu)/T} + 1}\right]\right\}.
\end{aligned}
\tag{24}
$$

For u, d and s quarks, polarization loops are obtained as

$$\Pi^{ps}_{f\bar{f}}(p_0 = m) = \frac{\beta N_c}{(2\pi)^2} \sum_{n,s} \int dk_z \frac{1}{E_{fns}} \left[1 - \frac{1}{e^{(E_{fns}-\mu)/T}+1} - \frac{1}{e^{(E_{fns}+\mu)/T}+1}\right]$$
$$+ p_0^2 \frac{\beta N_c}{(2\pi)^2} \sum_{n,s} \int dk_z \frac{1}{E_{fns}} \frac{1}{4E_{fns}^2 - p_0^2} \left[1 - \frac{1}{e^{(E_{fns}-\mu)/T}+1} - \frac{1}{e^{(E_{fns}+\mu)/T}+1}\right]. \quad (25)$$

The detailed derivation of polarization loops is given in the Appendix A.

III. RESULTS AND ANALYSIS

Due to NJL model is nonrenormalizable, a proper regularization scheme is needed. We adopt Pauli -Villars regularization [74] in the article. Any function containing M_f is replaced by a summation as

$$f(M_f) \to f_{p,V}(M_f) = \sum_{i=0}^{3} c_i \sqrt{{M_f}^2 + i\Lambda^2}, \quad (26)$$

where $c_0 = 1, c_1 = -3, c_2 = 3, c_3 = -1$. The parameter set is chosen as $m_{u,d} = 10.3$ MeV, $m_s = 236.9$ MeV, $\Lambda = 781.2$ MeV, $G\Lambda^2 = 4.90$, $K\Lambda^5 = 129.8$ [75]. We have considered one set of constant values of AMM with $\kappa_u = 0.123$, $\kappa_d = 0.555$, $\kappa_s = 0.329$.

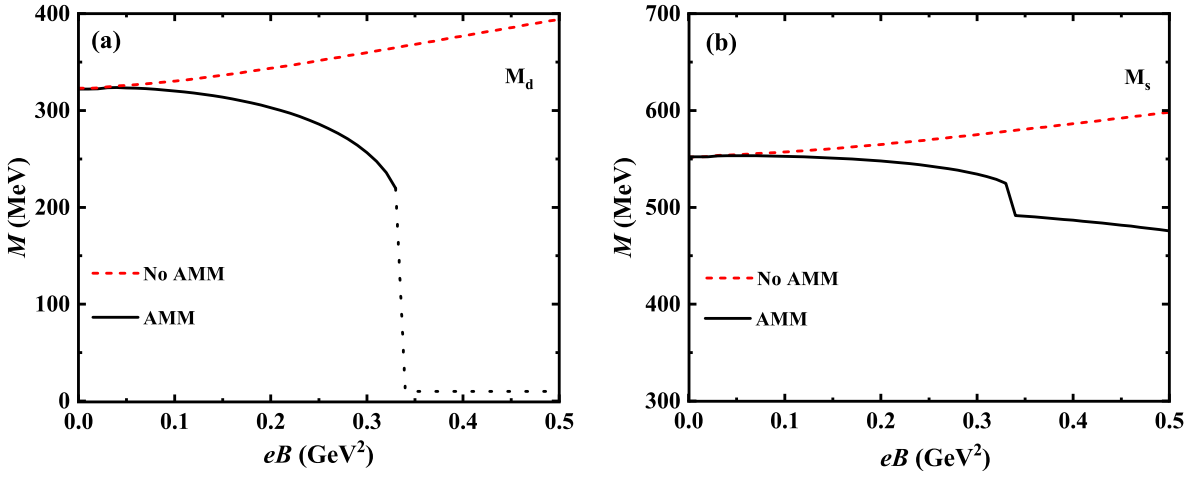

FIG. 1. The dependence of dynamical quark mass (M) on magnetic field (eB) with and without values of AMM at zero temperature. (a) and (b) are for d quark and s quark, respectively.

Figure 1 illustrates the dependence of the dynamical quark masses of d quarks and s quarks on the magnetic field at temperature $T = 0$. The study found that, without

considering the anomalous magnetic moment (AMM), the masses of both d quarks and s quarks increase with the enhancement of the magnetic field. However, when the AMM is taken into account, a novel phenomenon is observed, where the quark masses exhibit non-monotonic behavior with increasing magnetic field strength. It is observed that their mass increases with the enhancement of the magnetic field for d quarks. But when the magnetic field strength reaches $eB = 0.04$ GeV^2, their mass begins to decrease with the increase of the magnetic field, which is also shown the inverse magnetic catalysis (IMC) feature. When the magnetic field strength increases to $eB = 0.33$ GeV^2, the dynamical mass of d quarks drops sharply, directly to its current quark mass, indicating a first-order phase transition in the mass of light quarks. For s quark, its dynamical mass also exhibits non-monotonic behavior with the enhancement of the magnetic field, starting to decrease when the magnetic field strength increases to $eB = 0.06$ GeV^2. Within the entire range of magnetic fields considered, no first-order phase transition occurs for s quarks.

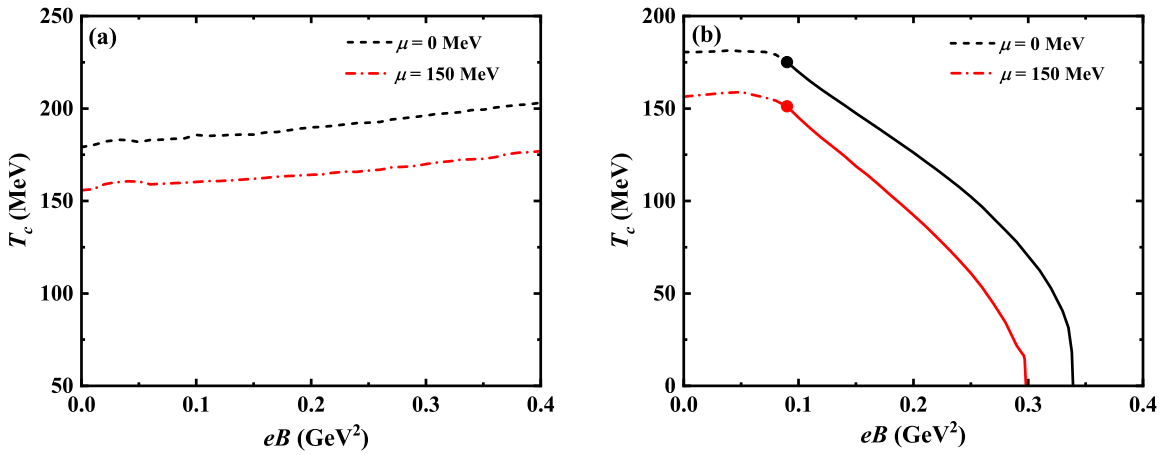

FIG. 2. The critical temperatures (T_c) for chiral phase transition as a function of the magnetic field for different chemical potentials without, on panel (a) and with quark AMM, on panel (b), respectively. The solid lines correspond to chiral first-order transition, the full dots correspond to CEP, and the other lines correspond to chiral crossover phase transition.

The critical temperature of chiral phase transition is determined by the peak value of the derivative of chiral condensate with respect to temperature. As can be seen from Fig. 2(a), when the AMM is not considered, the phase transition temperature increases with the increase of magnetic field, exhibiting magnetic catalysis for different chemical potentials.

However, the situation becomes completely different when the AMM is introduced. As shown in Fig. 2(b), it can be observed that the magnetic field has an inhibitory effect on the phase transition temperature T_c, exhibiting inverse magnetic catalysis characteristics. Furthermore, we have also discovered that for different chemical potentials in the $(T_c - eB)$ phase diagram, there exist critical endpoints (CEP) of phase transition. The critical endpoint (CEP) in the phase transition refers to the point where the first-order phase boundary and the crossover phase boundary intersect on the quantum chromodynamics (QCD) phase diagram. This point marks the transition of the phase transition nature, from a first-order phase transition (discontinuous physical quantities) to a crossover phase transition (continuous physical quantity changes but with a critical point). The study found that on the temperature-magnetic field $(T_c - eB)$ plane, as the magnetic field increases, the order of phase transition changes from a crossover phase transition to a first-order phase transition, and the critical endpoint (CEP) on the $(T_c - eB)$ plane is shown in Fig. 2(b). We also discussed the influence of AMM on the $(T_c - eB)$ phase diagram and found that introducing AMM leads to a decrease in the phase transition temperature T_c, but an increase in the critical temperature of the CEP.

Our analysis indicates that, except in the weak magnetic field region ($eB < 0.05$ GeV^2 at $\mu = 0$ MeV and $eB < 0.08$ GeV^2 at $\mu = 150$ MeV), the critical temperature of the chiral phase transition (whether it is a crossover or first-order transition) decreases with increasing magnetic field strength, indicating the phenomenon of inverse magnetic catalysis (IMC). Notably, the chiral phase transition exhibits crossover behavior in weak magnetic fields, regardless of zero or finite chemical potential, but evolves into a first-order transition in strong magnetic fields. For μ =0 MeV, the CEP is located at $eB = 0.09$ GeV^2, $T = 175.1$ MeV, while for μ =150 MeV, the CEP point moves to eB =0.09 GeV^2, $T = 151.2$ MeV.

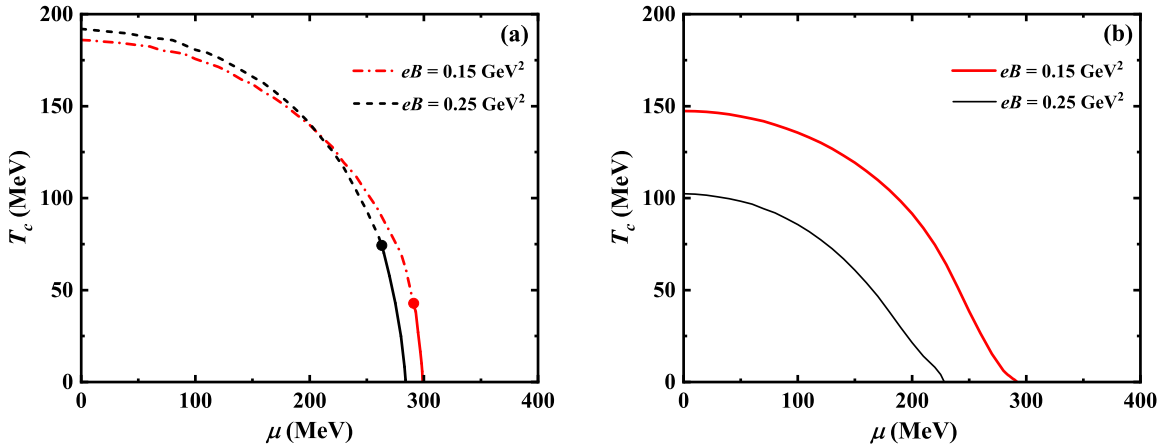

FIG. 3. The critical temperatures (T_c) for chiral phase transition as a function of chemical potential for different magnetic fields. Panel (a) is for without considering quark AMM, and panel (b) is for considering quark AMM. The solid lines correspond to chiral first-order transition, the full dots correspond to CEP, and the other lines correspond to chiral crossover phase transition.

Fig. 3 illustrates the $(T_c - \mu)$ phase diagram with different magnetic fields ($eB = 0.15$ GeV^2 and 0.25 GeV^2) without (a) and with (b) the quark AMM. Solid and dashed lines represent first-order and crossover phase transitions, respectively, with critical endpoints (CEPs) clearly marked. Fig. 3(b) shows that with the introduction of quark AMM, the $(T_c - \mu)$ phase diagram clearly exhibits first-order phase transition for the magnetic fields of $eB = 0.15$ GeV^2 and 0.25 GeV^2, respectively. This is in stark contrast to the case as shown in Fig. 3(a) where AMM is excluded, where the crossover phase transitions exist in the high temperature and low chemical potential region, and the first-order transitions exist in the low temperature and high chemical potential region. The critical endpoints without AMM, are located at $\mu_{\rm CEP} \approx 291.2$ MeV, $T_{\rm CEP} = 42.6$ MeV for $eB = 0.15$ GeV^2, and at $\mu_{\rm CEP} \approx 263.3$ MeV, $T_{\rm CEP} = 74.1$ MeV for $eB = 0.25$ GeV^2. Without considering AMM, the phase diagram aligns with conventional NJL predictions: magnetic fields strengthen chiral symmetry breaking (MC), and the crossover-to-first-order transition reflects competition between thermal and density effects. The CEP existence highlights the interplay of T and μ in driving chiral restoration.

As shown in Fig. 3(b) by considering AMM, it is found that AMM suppresses chiral symmetry breaking, reducing T_c and destabilizing the crossover regime. Quark masses exhibit

abrupt drops (shown in Fig.1) due to AMM-magnetic field coupling, favoring first-order transitions. The $u-d$ quark mass asymmetry amplifies under AMM, reshaping the phase boundaries. We firstly demonstrate in the SU(3) NJL model that AMM eliminates crossover transitions, universalizing first-order chiral transitions under magnetic fields. It is found that AMM couples to magnetic fields to suppress T_c, resolving discrepancies between NJL predictions and LQCD results [16, 22–27, 73].

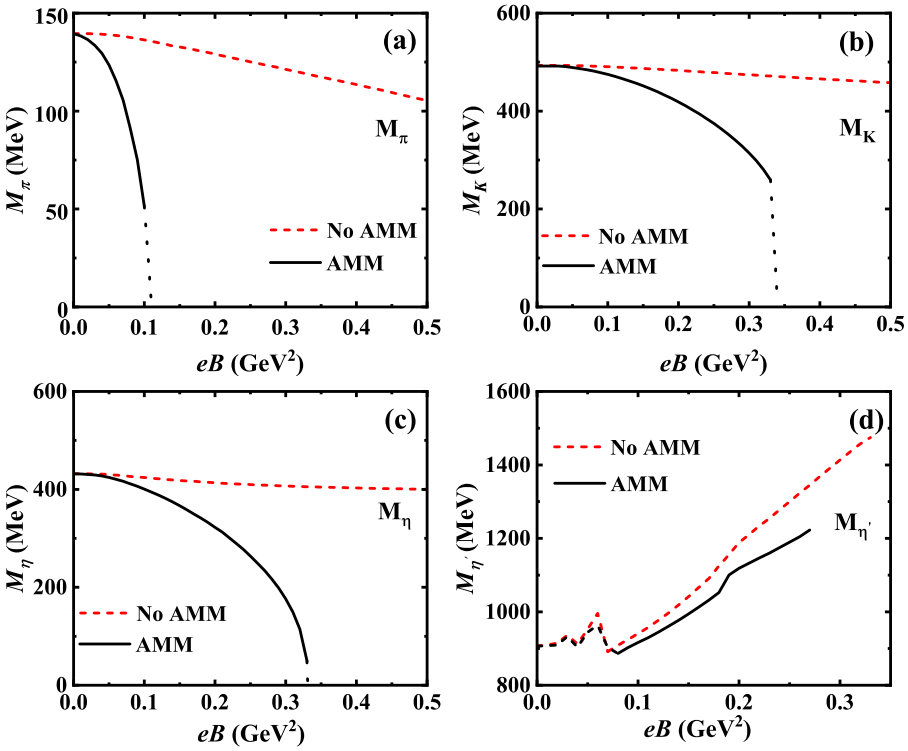

FIG. 4. The magnetic field dependence of neutral pseudoscalar meson masses (π, K, η, η') at zero temperature, comparing cases with and without the inclusion of quark anomalous magnetic moments (AMM). Panels (a), (b), (c) and (d) are for π, K, η and η', respectively.

Fig. 4 illustrates the magnetic field dependence of neutral pseudoscalar meson masses (π, K, η, η') at zero temperature, comparing cases with and without the inclusion of quark anomalous magnetic moments (AMM). As shown in Fig. 4(a), it is found that the π meson mass decreases slightly with increasing magnetic field (eB), reflecting mild suppression due to magnetic catalysis (MC) without AMM. But the π mass drops sharply and collapses to zero at a critical magnetic field $eB_c \approx 0.1$ GeV^2, signaling a first-order phase transition with

AMM. It is manifested that the π meson, composed of light (u/d) quarks, is highly sensitive to AMM. The abrupt mass collapse indicates that AMM destabilizes chiral symmetry breaking, directly linking π stability to non-perturbative quark dynamics under strong magnetic fields.

As shown in Fig. 4(b), it is found that the K meson mass decreases gradually but remains finite across the studied eB range without considering AMM. But the K mass declines more steeply and vanishes at $eB_{\rm c} \approx 0.33$ GeV^2 with AMM, i.e the critical magnetic field of the K meson similarly occurs in the vicinity of the quarks' first-order phase transitions at $eB_{\rm c} \approx 0.33$ GeV^2. It is manifested that the K meson s-quark component reduces its sensitivity to AMM compared to π. However, AMM enhances the coupling between light (u/d) and strange quarks, accelerating chiral symmetry restoration for K at higher eB.

The η mass decreases slowly, maintaining a smooth trend without AMM as shown in 4(c). But a rapid mass reduction occurs with AMM, culminating in a sharp drop to zero at $eB_{\rm c} \approx 0.33$ GeV^2, similar to the K meson. It is manifested that the η meson mixed flavor structure (η_0 and η_8 states) makes its mass sensitive to both light and strange quark dynamics. AMM-induced isospin symmetry breaking amplifies η coupling to the magnetic field, leading to a faster chiral restoration. As shown in Fig. 4(d), the η' mass increases monotonically with eB but becomes undefined above $eB_c \approx 0.33$ GeV^2 due to divergences in polarization loops without AMM. Even with the introduction of AMM, the η' mass still increases, but the magnitude is suppressed, and the solution is lost at a lower $eB_c \approx 0.27$ GeV^2. The η' meson, regarded as a resonance state in the NJL model, exhibits strong sensitivity to the η' decay width. AMM exacerbates the limitations of the model by enhancing non-perturbative decay effects, thus restricting its physical solutions in strong fields.

In the critical magnetic field eB, AMM can trigger a sudden mass collapse (for example, π, K, η), which does not occur in the smooth trend without AMM. AMM lowers the threshold $eB_{\rm c}$ for phase transitions (for example, π: 0.1 GeV^2 compared to a higher eB without AMM). AMM disrupts the stability of mesons by enhancing the non-monotonicity of quark masses, especially for states dominated by light flavors (π, K, η).

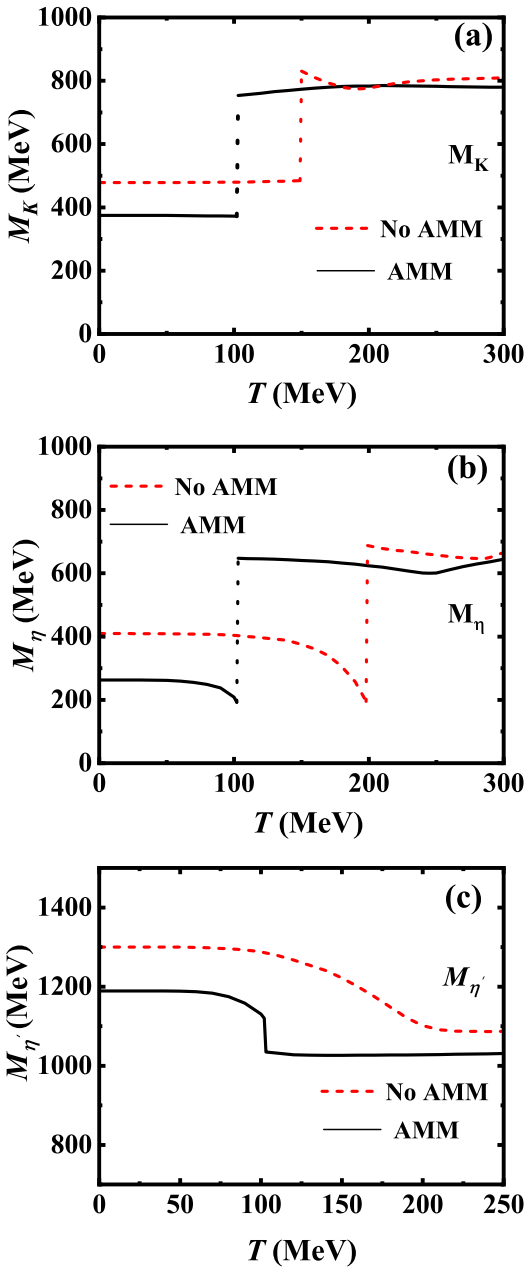

FIG. 5. K, η and η' meson masses as a function of temperature for without and with considering AMM. Panels (a), (b) and (c) are for K, η and η', respectively.

Fig. 5 depicts the temperature dependence of neutral pseudoscalar meson masses (K,η and η') under a constant magnetic field ($eB_c = 0.25$ GeV^2), comparing scenarios with and without AMM. As shown in Fig. 5(a), the K meson mass increases slightly with temperature

until reaching the Mott temperature ($T_{\rm mott} \approx 149$ MeV), where it undergoes a discontinuous jump without considering AMM. This marks the transition from a bound state to a resonance state. Beyond T_{mott} , the mass first decreases slightly, then rises again at $T \sim 190$ MeV. But when considering AMM, the K mass decreases slightly with temperature at low T (¡102 MeV), contrasting the AMM-free case. A sharp mass jump occurs at the first-order phase transition temperature of light quarks (u/d), followed by a gradual increase until $T \sim 216$ MeV, after which the mass declines. The AMM destabilizes the K meson by coupling light quark dynamics to the magnetic field. The first-order quark mass drop directly triggers the K mass jump, replacing the smooth Mott transition seen without AMM.

As shown in Fig. 5(b), it is found that the η mass decreases slowly with T until $T_{\rm mott} \approx$ 198 MeV, where a mass jump occurs without considering AMM. Then the mass continues to decline before rising again at $T \sim 284$ MeV. But when considering AMM, the η mass drops abruptly at the light quark first-order transition temperature, followed by a gradual decrease. At $T \sim 247$ MeV, the mass begins to rise. At high T, the η mass is systematically lower than in the AMM-free case. The η meson mixed flavor composition (combining light and strange quarks) makes it sensitive to both u/d-quark phase transitions and AMM-enhanced magnetic effects. AMM shifts the mass jump to lower T, reflecting stronger chiral symmetry restoration.

As shown in Fig. 5(c), it is found that the η' mass decreases monotonically with T until $T \sim 235$ MeV without considering AMM, after which it begins to rise. But when considering AMM, the η' mass decreases initially, exhibits a sudden drop (~ 100 MeV) at the light quark first-order transition ($T \sim 102$ MeV), then rises slightly at $T > 151$ MeV. The overall mass reduction is more pronounced compared to the AMM-free case. Similarly as a resonance state in the NJL model, the η' is highly sensitive to it's resonance state decay widths. AMM amplifies non-perturbative effects, destabilizing the η' through enhanced decay widths and coupling to light quark phase transitions.

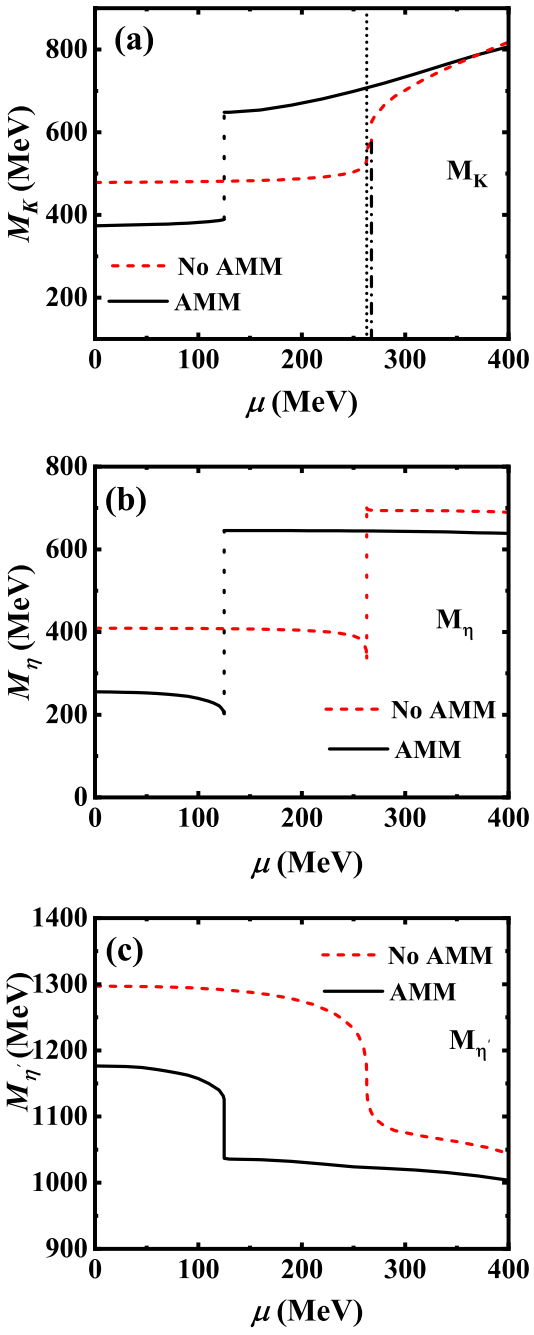

FIG. 6. The dependence of the masses of neutral pseudoscalar mesons (K, η and η') on the quark chemical potential (μ) under a fixed temperature ($T = 75$ MeV) and magnetic field ($eB_c = 0.25$ GeV^2). Panels (a), (b) and (c) are for K, η and η', respectively.

Fig. 6 illustrates the dependence of the masses of neutral pseudoscalar mesons (K, η

and $\eta^{'}$) on the quark chemical potential (μ) under a fixed temperature ($T = 75$ MeV) and magnetic field ($eB_c = 0.25$ GeV^2), comparing scenarios with and without the inclusion of quark anomalous magnetic moments (AMM). As shown in Fig. 6(a), it is found that the K-meson mass increases continuously with μ, exhibiting a steep rise near the critical endpoint (CEP) at $\mu_{\rm CEP} \approx 262.8$ MeV without considering AMM. A Mott transition (discontinuous jump) occurs at $\mu > \mu_{\rm CEP}$, marking the transition from a bound state to a resonance state. But when considering AMM, the K-meson undergoes an abrupt Mott transition directly at $\mu_{\rm CEP}({\rm AMM}) \approx 124.9$ MeV, reflecting a first-order chiral phase transition induced by AMM. This shift highlights how AMM destabilizes the K-meson by coupling light quark dynamics to the magnetic field, accelerating chiral symmetry restoration.

As shown in Fig. 6(b), it is found that the η-meson mass decreases smoothly with μ, interrupted by a mass jump at $\mu_{\rm CEP}$ without considering AMM. But when considering AMM, the mass jump shifts to $\mu_{\rm CEP}({\rm AMM})$, followed by a continued decline. The mixed flavor composition of η (combining light and strange quarks) makes it sensitive to both u/d-quark phase transitions and AMM-enhanced magnetic effects. AMM amplifies isospin symmetry breaking, accelerating mass reduction. As shown in Fig. 6(c), it is found that the η'-meson mass decreases monotonically with μ, with the steepest decline aligning with $\mu_{\rm CEP}$ without considering AMM. But when considering AMM, A sudden mass drop occurs at $\mu_{\rm CEP}({\rm AMM})$, followed by a gradual decline. Similarly as a resonance state, η' is highly sensitive to it's decay widths. AMM amplifies non-perturbative effects, destabilizing η' through enhanced decay widths and coupling to light quark phase transitions.

The shift from smooth crossovers to first-order transitions under AMM demonstrates how quark-level magnetic interactions reshape the QCD phase diagram. This provides insights into the competition between thermal, density, and magnetic effects in chiral symmetry restoration. By reproducing features like inverse magnetic catalysis (IMC) and aligning with lattice QCD trends, the inclusion of AMM improves the predictive power of effective models like NJL. It bridges gaps between theory and experiments, guiding future refinements for charged and vector meson studies.

IV. SUMMARY AND CONCLUSIONS

In this study, we systematically investigated the effects of quark anomalous magnetic moments (AMM) on the mass spectra of neutral pseudoscalar mesons (π, K, η, η') under external magnetic fields, finite temperatures, and quark chemical potentials within the framework of the three-flavor Nambu-Jona-Lasinio (NJL) model. By incorporating AMM at the quark level, we explored the interplay between magnetic catalysis (MC), inverse magnetic catalysis (IMC), and chiral symmetry restoration, addressing discrepancies between conventional NJL predictions and lattice QCD (LQCD) results.

Key findings from our analysis include: (1) Quark Mass Dynamics: The inclusion of AMM significantly alters the magnetic field dependence of constituent quark masses. For light quarks (u/d), a first-order phase transition emerges at critical magnetic fields ($eB_{\rm c} \approx 0.10$ GeV^2), where their dynamical masses collapse to current quark masses. In contrast, the strange quark exhibits non-monotonic mass behavior but avoids abrupt transitions. These results highlight the critical role of AMM in destabilizing chiral condensates and driving IMC. (2) Phase Diagram Modifications: The introduction of AMM reshapes the QCD phase structure. At finite chemical potential (μ), AMM suppresses the chiral phase transition temperature ($T_{\rm c}$) and shifts critical endpoints (CEP) toward lower μ and T. Notably, crossover transitions observed in the absence of AMM are replaced by first-order transitions under strong magnetic fields, aligning more closely with LQCD findings on IMC. (3) Meson Mass Behavior: The π mass collapses abruptly at $eB_{\rm c} \approx 0.10$ GeV^2 with AMM, signaling a direct link between light quark dynamics and chiral symmetry restoration. K and η Mesons both exhibit mass reductions and sharp transitions at higher $eB(\sim 0.33$ GeV$^2)$, governed by thresholds tied to strange quark mass ($2m_s$). AMM enhances flavor mixing and accelerates chiral restoration. η' Meson: As a resonance state, η' shows suppressed mass growth under AMM and loses stability at strong fields ($eB \geq 0.27$ GeV^2), reflecting limitations of the NJL framework in handling non-perturbative decay widths. (4) Temperature and Chemical Potential Dependence: At finite T and μ, AMM induces discontinuous mass jumps in mesons (e.g., K, η) at first-order phase transitions, replacing smooth Mott transitions. These jumps correlate with abrupt drops in light quark masses, emphasizing the role of AMM in mediating magnetic-thermal-density couplings.

Our results demonstrate that AMM plays a pivotal role in reconciling NJL model predic-

tions with LQCD observations, particularly in reproducing IMC and non-monotonic phase boundaries. However, challenges remain in fully capturing the η' meson behavior, underscoring the need to incorporate decay widths and beyond-RPA corrections. Future work will extend this framework to charged and vector mesons, which are crucial for understanding electromagnetic probes in heavy-ion collisions and magnetar environments. Additionally, refining the interplay between AMM and the $U_A(1)$ anomaly could further elucidate the chiral and axial restoration mechanisms in magnetized QCD matter.

ACKNOWLEDGMENTS

This work was supported by the National Natural Science Foundation of China (Grants No. 11875178, No. 11475068, No. 11747115).

Appendix A: THE CALCULATION OF POLARIZATION LOOPS

In this appendix, we derive the main part of the polarization function containing the quark AMM at finite temperature. We start with the following expression using kaon meson as an example

$$\int \frac{d^4k}{(2\pi)^4} Tr\{\gamma^5 S_d(q=p+k)\gamma^5 S_s(k)\}. \tag{A1}$$

Substitute Eq. (21) into Eq. (A1) and doing the trace operation on the gamma matrix, we get,

$$\begin{aligned}
&\int \frac{d^4k}{(2\pi)^4} \mathrm{Tr}\left\{\gamma^5 S_d(q=p+k)\gamma^5 S_s(k)\right\} \\
&= \int \frac{d^4k}{(2\pi)^4}\, 2e^{-\frac{q_\perp^2}{|e_dB|}-\frac{k_\perp^2}{|e_sB|}} \sum_{n,m,s,l} (-1)^{n+m} \frac{1}{M_{nd}M_{ms}} \left[(-q_0k_0+q_zk_z)+(sM_{nd}-\kappa_d e_dB)(lM_{ms}-\kappa_s e_sB)\right] \\
&\quad\times \Bigg\{ (M_{nd}+sM_d)(M_{ms}+lM_s) L_n\left(\frac{2q_\perp^2}{|e_dB|}\right) L_m\left(\frac{2k_\perp^2}{|e_sB|}\right) \\
&\quad + (M_{nd}-sM_d)(M_{ms}-lM_s) L_{n-1}\left(\frac{2q_\perp^2}{|e_dB|}\right) L_{m-1}\left(\frac{2k_\perp^2}{|e_sB|}\right) \\
&\quad + 8ls(q_xk_x+q_yk_y) L_{n-1}^1\left(\frac{2q_\perp^2}{|e_dB|}\right) L_{m-1}^1\left(\frac{2k_\perp^2}{|e_sB|}\right) \Bigg\}\times \\
&\quad \left\{\frac{1}{q_0^2-E_{dns}^2+i\epsilon}+2\pi i n_F(q_0)\delta(q_0^2-E_{dns}^2)\right\}\left\{\frac{1}{k_0^2-E_{sml}^2+i\epsilon}+2\pi i n_F(k_0)\delta(k_0^2-E_{sml}^2)\right\}.
\end{aligned} \tag{A2}$$

Now considering $\vec{p}=0$, and using the orthogonality relation of the Laguerre function

$$\int_0^\infty dx e^{-x}x^\alpha L_n^\alpha(x)L_m^\alpha(x)=\frac{\Gamma(\alpha+n+1)}{n!}, m=n, \mathrm{Re}\,\alpha>0. \tag{A3}$$

We arrive at

$$\begin{aligned}
&\int \frac{d^4k}{(2\pi)^4}Tr\{\gamma^5 S_d(q=p+k)\gamma^5 S_s(k)\}\\
&=-\frac{N_c}{(2\pi)^2}\sum_{n,s,l}\int\frac{dk_0dk_z}{2\pi}\frac{1}{M_{nd}}\frac{1}{M_{ns}}\beta\left[(-q_0k_0+k_zk_z)+(sM_{nd}-\kappa_d e_d B)(lM_{ns}-\kappa_s e_s B)\right]\times\\
&\left[(M_{nd}+sM_d)(M_{ns}+lM_s)+(M_{nd}-sM_d)(M_{ns}-lM_s)+4ls\beta n\right]\times\\
&\left\{\frac{1}{q_0^2-{E_{dns}}^2+i\varepsilon}+2\pi i n_F(q_0)\delta(q_0^2-{E_{dns}}^2)\right\}\left\{\frac{1}{k_0^2-{E_{snl}}^2+i\varepsilon}+2\pi i n_F(k_0)\delta(k_0^2-{E_{snl}}^2)\right\}.
\end{aligned}\tag{A4}$$

Performing the dk_0 integral of Eq.(A4), we get

$$\begin{aligned}
&\Pi^{ps}_{K^0}(p_0=m_{K^0})=\frac{\beta N_c}{2(2\pi)^2}\sum_{n,s,l}(1+sl\frac{M_dM_s+2\beta n}{M_{nd}M_{ns}})\\
&\left\{\int dk_z\frac{1}{E_{dns}}\left[1-\frac{1}{e^{(E_{dns}-\mu)/T}+1}-\frac{1}{e^{(E_{dns}+\mu)/T}+1}\right]+\int dk_z\frac{1}{E_{snl}}\left[1-\frac{1}{e^{(E_{snl}-\mu)/T}+1}-\frac{1}{e^{(E_{snl}+\mu)/T}+1}\right]\right.\\
&\left.+\left\{[(M_{nd}-s\kappa_d e_d B)-sl(M_{ns}-l\kappa_s e_s B)]^2-p_0^2\right\}B(m_d,m_d)\right\},
\end{aligned}\tag{A5}$$

where,

$$\begin{aligned}
&B(m_d,m_s)=\\
&\int dk_z\left\{\frac{1}{E_{dns}}\left[\frac{1}{(E_{dns}+p_0)^2-{E_{snl}}^2}\frac{1}{e^{-(E_{dns}+\mu)/T}+1}-\frac{1}{(E_{dns}-p_0)^2-{E_{snl}}^2}\frac{1}{e^{-(E_{dns}-\mu)/T}+1}\right]\right.\\
&\left.+\frac{1}{E_{snl}}\left[\frac{1}{(E_{snl}-p_0)^2-{E_{dns}}^2}\frac{1}{e^{-(E_{snl}+\mu)/T}+1}-\frac{1}{(E_{snl}+p_0)^2-{E_{dns}}^2}\frac{1}{e^{(E_{snl}-\mu)/T}+1}\right]\right\}.
\end{aligned}\tag{A6}$$

---

[1] D. Grasso and H. R. Rubinstein, Phys. Rept. **348**, 163 (2001).

[2] T. Vachaspati, Phys. Lett. B **265**, 258 (1991).

[3] R. C. Duncan and C. Thompson, Astrophys. J. Lett. **392**, L9 (1992).

[4] D. Lai and S. L. Shapiro, Astrophysical Journal, Part 1 (ISSN 0004-637X), vol. 383, Dec. 20, 1991, p. 745-751. **383**, 745 (1991).

[5] K. Tuchin, Adv. High Energy Phys. **2013**, 490495 (2013).

[6] V. Skokov, A. Y. Illarionov, and V. Toneev, Int. J. Mod. Phys. A **24**, 5925 (2009).

[7] Y. Guo, S. Shi, S. Feng, and J. Liao, Phys. Lett. B **798**, 134929 (2019).

[8] D. She, S.-Q. Feng, Y. Zhong, and Z.-B. Yin, Eur. Phys. J. A **54**, 48 (2018).

[9] Y. Zhong, C.-B. Yang, X. Cai, and S.-Q. Feng, Chin. Phys. C **39**, 104105 (2015).

[10] W.-T. Deng and X.-G. Huang, Phys. Rev. C **85**, 044907 (2012).

[11] B.-X. Chen and S.-Q. Feng, Chin. Phys. C **44**, 024104 (2020).

[12] I. A. Shovkovy, Lect. Notes Phys. **871**, 13 (2013).

[13] F. Preis, A. Rebhan, and A. Schmitt, Lect. Notes Phys. **871**, 51 (2013).

[14] K. Fukushima, Lect. Notes Phys. **871**, 241 (2013).

[15] D. E. Kharzeev, Prog. Part. Nucl. Phys. **75**, 133 (2014).

[16] G. S. Bali, F. Bruckmann, G. Endrodi, Z. Fodor, S. D. Katz, S. Krieg, A. Schafer, and K. K. Szabo, JHEP **02**, 044 (2012).

[17] M. D'Elia, S. Mukherjee, and F. Sanfilippo, Phys. Rev. D **82**, 051501 (2010).

[18] M. D'Elia and F. Negro, Phys. Rev. D **83**, 114028 (2011).

[19] V. P. Gusynin, V. A. Miransky, and I. A. Shovkovy, Phys. Rev. Lett. **73**, 3499 (1994), [Erratum: Phys.Rev.Lett. 76, 1005 (1996)].

[20] V. P. Gusynin, V. A. Miransky, and I. A. Shovkovy, Phys. Rev. D **52**, 4718 (1995).

[21] V. P. Gusynin, V. A. Miransky, and I. A. Shovkovy, Phys. Lett. B **349**, 477 (1995).

[22] H.-T. Ding, C. Schmidt, A. Tomiya, and X.-D. Wang, Phys. Rev. D **102**, 054505 (2020).

[23] G. S. Bali, F. Bruckmann, G. Endrodi, Z. Fodor, S. D. Katz, and A. Schafer, Phys. Rev. D **86**, 071502 (2012).

[24] E. M. Ilgenfritz, M. Muller-Preussker, B. Petersson, and A. Schreiber, Phys. Rev. D **89**, 054512 (2014).

[25] V. G. Bornyakov, P. V. Buividovich, N. Cundy, O. A. Kochetkov, and A. Schäfer, Phys. Rev. D **90**, 034501 (2014).

[26] G. S. Bali, F. Bruckmann, G. Endrődi, S. D. Katz, and A. Schäfer, JHEP **08**, 177 (2014).

[27] A. Tomiya, H.-T. Ding, X.-D. Wang, Y. Zhang, S. Mukherjee, and C. Schmidt, arXiv preprint arXiv:1904.01276 (2019).

[28] J. O. Andersen, W. R. Naylor, and A. Tranberg, Rev. Mod. Phys. **88**, 025001 (2016).

[29] M. Ruggieri, L. Oliva, P. Castorina, R. Gatto, and V. Greco, Phys. Lett. B **734**, 255 (2014).

[30] M. Ferreira, P. Costa, O. Lourenço, T. Frederico, and C. Providência, Phys. Rev. D **89**, 116011 (2014).

[31] R. L. S. Farias, V. S. Timoteo, S. S. Avancini, M. B. Pinto, and G. Krein, Eur. Phys. J. A **53**, 101 (2017).

[32] X. Zhu and S.-Q. Feng, Phys. Rev. D **107**, 016018 (2023).

[33] S. Fayazbakhsh and N. Sadooghi, Phys. Rev. D **90**, 105030 (2014).

[34] Y.-W. Qiu, S.-Q. Feng, and X.-Q. Zhu, Phys. Rev. D **108**, 116022 (2023).

[35] S. Mao, Phys. Lett. B **758**, 195 (2016).

[36] E. J. Ferrer, V. de la Incera, I. Portillo, and M. Quiroz, Phys. Rev. D **89**, 085034 (2014).

[37] L. Chang, Y.-X. Liu, and C. D. Roberts, Phys. Rev. Lett. **106**, 072001 (2011).

[38] E. J. Ferrer and V. de la Incera, Phys. Rev. Lett. **102**, 050402 (2009).

[39] S. Mao and D. H. Rischke, Phys. Lett. B **792**, 149 (2019).

[40] J. Mei and S. Mao, Phys. Rev. D **102**, 114035 (2020).

[41] E. J. Ferrer and V. de la Incera, Nucl. Phys. B **824**, 217 (2010).

[42] P. J. A. Bicudo, J. E. F. T. Ribeiro, and R. Fernandes, Phys. Rev. C **59**, 1107 (1999).

[43] J. O. Andersen, Phys. Rev. D **86**, 025020 (2012).

[44] K. Kamikado and T. Kanazawa, JHEP **03**, 009 (2014).

[45] G. a. Krein and C. Miller, Symmetry **13**, 551 (2021).

[46] K. Xu, J. Chao, and M. Huang, Phys. Rev. D **103**, 076015 (2021).

[47] Z. Wang and P. Zhuang, Phys. Rev. D **97**, 034026 (2018).

[48] M. Coppola, D. Gómez Dumm, and N. N. Scoccola, Phys. Lett. B **782**, 155 (2018).

[49] R. Zhang, W.-j. Fu, and Y.-x. Liu, Eur. Phys. J. C **76**, 307 (2016).

[50] H. Liu, X. Wang, L. Yu, and M. Huang, Phys. Rev. D **97**, 076008 (2018).

[51] J. Li, G. Cao, and L. He, Phys. Rev. D **104**, 074026 (2021).

[52] S. Mao, Phys. Rev. D **99**, 056005 (2019).

[53] G. Colucci, E. S. Fraga, and A. Sedrakian, Phys. Lett. B **728**, 19 (2014).

[54] B. Sheng, Y. Wang, X. Wang, and L. Yu, Phys. Rev. D **103**, 094001 (2021).

[55] D. Gómez Dumm, M. F. Izzo Villafañe, and N. N. Scoccola, Phys. Rev. D **97**, 034025 (2018).

[56] S. S. Avancini, R. L. S. Farias, and W. R. Tavares, Phys. Rev. D **99**, 056009 (2019).

[57] L. Li and S. Mao, Chin. Phys. C **46**, 094105 (2022).

[58] T. Kojo, Eur. Phys. J. A **57**, 317 (2021).

[59] A. Mishra and S. P. Misra, Int. J. Mod. Phys. E **30**, 2150014 (2021).

[60] G. 't Hooft, Phys. Rev. D **14**, 3432 (1976), [Erratum: Phys.Rev.D 18, 2199 (1978)].

[61] G. 't Hooft, Phys. Rept. **142**, 357 (1986).

[62] T. Kunihiro and T. Hatsuda, Phys. Lett. B **206**, 385 (1988), [Erratum: Phys.Lett.B 210, 278–278 (1988)].

[63] H. Reinhardt and R. Alkofer, Phys. Lett. B **207**, 482 (1988).

[64] V. Bernard, R. L. Jaffe, and U. G. Meissner, Nucl. Phys. B **308**, 753 (1988).

[65] Y. Nambu and G. Jona-Lasinio, Phys. Rev. **122**, 345 (1961).

[66] Y. Nambu and G. Jona-Lasinio, Phys. Rev. **124**, 246 (1961).

[67] S. P. Klevansky, Rev. Mod. Phys. **64**, 649 (1992).

[68] M. K. Volkov, Phys. Part. Nucl. **24**, 35 (1993).

[69] M. Buballa, Phys. Rept. **407**, 205 (2005).

[70] T. Hatsuda and T. Kunihiro, Phys. Rept. **247**, 221 (1994).

[71] P. Rehberg, S. P. Klevansky, and J. Hufner, Phys. Rev. C **53**, 410 (1996).

[72] P. Costa, M. C. Ruivo, C. A. de Sousa, and Y. L. Kalinovsky, Phys. Rev. D **71**, 116002 (2005).

[73] R. Aguirre, Phys. Rev. D **95**, 074029 (2017).

[74] W. Pauli and F. Villars, Rev. Mod. Phys. **21**, 434 (1949).

[75] S. Carignano and M. Buballa, Phys. Rev. D **101**, 014026 (2020).